JOURNAL OF VIROLOGY, July 2011, p. 6657–6668 Vol. 85, No. 13
0022-538X/11/$12.00 doi:10.1128/JVI.00302-11

Ambivalent Role of the Innate Immune Response in Rabies Virus Pathogenesis▽†

Damien Chopy,[1,2] Julien Pothlichet,[3,4]‡ Mireille Lafage,[1,2] Françoise Mégret,[1,2] Laurence Fiette,[5] Mustapha Si-Tahar,[3,4] and Monique Lafon[1,2]*

Institut Pasteur, Unité de Neuroimmunologie Virale, Département de Virologie, F-75015 Paris, France[1]; CNRS, URA3015, F-75015 Paris, France[2]; Institut Pasteur, Unité de Défense Innée et Inflammation, Département d'Infection et d'Epidémiologie, F-75015 Paris, France[3]; INSERM, U874, F-75015 Paris, France[4]; and Institut Pasteur, Unité d'Histopathologie Humaine et Modèles Animaux, F-75015 Paris, France[5]

Received 11 February 2011/Accepted 13 April 2011

The neurotropic rabies virus (RABV) has developed several evasive strategies, including immunoevasion, to successfully infect the nervous system (NS) and trigger a fatal encephalomyelitis. Here we show that expression of LGP2, a protein known as either a positive or negative regulator of the RIG-I-mediated innate immune response, is restricted in the NS. We used a new transgenic mouse model (LGP2 TG) overexpressing LGP2 to impair the innate immune response to RABV and thus revealed the role of the RIG-I-mediated innate immune response in RABV pathogenesis. After infection, LGP2 TG mice exhibited reduced expression of inflammatory/chemoattractive molecules, beta interferon (IFN-β), and IFN-stimulated genes in their NS compared to wild-type (WT) mice, demonstrating the inhibitory function of LGP2 in the innate immune response to RABV. Surprisingly, LGP2 TG mice showed more viral clearance in the brain and lower morbidity than WT mice, indicating that the host innate immune response, paradoxically, favors RABV neuroinvasiveness and morbidity. LGP2 TG mice exhibited similar neutralizing antibodies and microglia activation to those of WT mice but showed a reduction of infiltrating $CD4^+$ T cells and less disappearance of infiltrating $CD8^+$ T cells. This occurred concomitantly with reduced neural expression of the IFN-inducible protein B7-H1, an immunoevasive protein involved in the elimination of infiltrated $CD8^+$ T cells. Our study shows that the host innate immune response favors the infiltration of T cells and, at the same time, promotes $CD8^+$ T cell elimination. Thus, to a certain extent, RABV exploits the innate immune response to develop its immunoevasive strategy.

Rabies virus (RABV) is a negative-strand RNA virus that infects mainly neurons and exploits the nervous system (NS) network to ensure its progression from the site of entry (bite site) to the site of exit, the salivary glands. The virulence of RABV relies on several factors, such as its capacity to avoid premature death of infected neurons and its property of escaping the immune response. Different mechanisms have been proposed to explain the inefficiency of the immune response against RABV infection (24). RABV infection induces immune unresponsiveness (6, 53), limits T cell infiltration into the NS (44), and keeps the blood-brain barrier tightly closed (37, 45). It also promotes the destruction of migratory $CD8^+$ T cells in the NS through the upregulation of immunoevasive proteins such as B7-H1 (1, 27, 28). B7-H1 (also known as PD-1 ligand and CD274) is interferon (IFN) inducible and is usually expressed by immune cells. It contributes to dampening proliferation, cytokine production, and cytolytic activity (20, 28, 48).

During its migration in the NS, RABV has to deal with the first line of defense against pathogens: the host innate immune response. RABV infection activates the innate immune sensor RIG-I, and likely also MDA-5 (15, 22), and triggers classical type I IFN, chemoattractive, and inflammatory responses in infected cells, which could be responsible for setting up an antiviral environment and triggering an efficient immune response (3, 9, 15, 25, 39, 41, 58). Like most viruses, RABV has developed a strategy to counteract the antiviral effect of the type I IFN response (23, 34, 40, 41, 55, 56). Despite these mechanisms, IFN, chemoattractive, and inflammatory responses in the RABV-infected NS are far from abrogated, and RABV successfully infects the NS (28, 58).

In this study, we investigate to what extent the innate immune response in the NS is important for the efficiency of RABV, immunoevasive strategy, and pathogenesis. To disturb the innate immune response and thus reveal its role in RABV infection, we infected a new mouse transgenic model that overexpresses LGP2 (LGP2 TG) with a neurovirulent RABV strain. LGP2 has been described as either a negative or positive regulator of RIG-I-like receptor-mediated immune responses (38, 42, 47). Several reports described LGP2 as a negative regulator of RIG-I signaling during infection with negative-strand RNA viruses, such as Sendai virus (SeV) or vesicular stomatitis virus (VSV) (38, 42). Three mechanisms have been proposed to explain the inhibitory function of LGP2 on RIG-I pathways: (i) LGP2 binds to viral double-stranded RNA (dsRNA) and prevents RIG-I recognition, (ii) LGP2 binds to RIG-I through a regulatory domain and inhibits RIG-I activation and interaction with IPS-1, and (iii) LGP2 competes with IKK epsilon for binding to and activation of IPS-1 (2, 31).

After demonstrating the negative function of LGP2 in the

* Corresponding author. Mailing address: Institut Pasteur, Unité de Neuroimmunologie Virale, Département de Virologie, F-75015 Paris, France. Phone: 33 1 45 68 87 52. Fax: 33 1 40 61 33 12. E-mail: monique.lafon@pasteur.fr.

‡ Present address: McGill University, Department of Human Genetics, H3G 0B1 Montréal, Québec, Canada.

▽ Published ahead of print on 27 April 2011.

† The authors have paid a fee to allow immediate free access to this article.

innate immune response during RABV infection both *in vitro* and in the NS, we showed that LGP2 expression is restricted in neuronal cells. The impairment of the innate immune response in the NS of transgenic mice makes LGP2 TG mice a proper model to study the contribution of the RIG-I-mediated innate immune response to RABV pathogenesis. We compared wild-type (WT) and LGP2 TG mice for morbidity and mortality, T cell infiltration, drop of migratory $CD8^+$ T cells, and B7-H1 expression in the NS (T cell destruction and B7-H1 overexpression are two features of RABV's immunoevasive strategy). We showed that impairment of the innate immune response leads to lower morbidity but has no effect on mortality during RABV infection. The innate immune response impairment slows down T cell infiltration, prevents RABV's immunoevasive strategy, and favors RABV elimination from the brain. Thus, RABV may exploit the host innate immune response to successfully invade the NS of the infected host.

MATERIALS AND METHODS

Cells and virus. Mouse NIH 3T3 fibroblasts and dorsal root ganglia, as well as SKNSH human neuroblastoma cells (ATCC HTB11), embryonic kidney cells (Hek293A) (QBiogene), and postmitotic neurons (NT2N), were prepared and grown as previously described (8, 29, 39). The laboratory RABV strain CVS (CVS-NIV), a highly pathogenic strain causing fatal encephalomyelitis in mice after intramuscular injection (7), and SeV were propagated as previously described (50, 52). Cells were infected at a multiplicity of infection of 3 and cultivated at 37°C in 5% CO_2.

Mice. Transgenic mice overexpressing human *LGP2* (LGP2 TG mice) were generated using C57BL/6 embryonic cells stably transduced at the one-cell stage with a lentiviral vector carrying *LGP2* (DHX58; GenBank accession no. NM_024119) under the control of the cytomegalovirus (CMV) early enhancer/chicken β-actin (CAG) promoter. Homozygous LGP2 TG mice were born at the Mendelian ratio. They developed and bred normally and had no obvious behavioral changes. Histology analysis performed on two male and two female 15-week-old LGP2 TG mice revealed no lesion or alteration in 17 distinct organs and tissues (including brain, cerebellum, spinal cord, heart, lung, liver, spleen, thymus, mesenteric lymph node, inguinal lymph node, superficial cervical lymph node, stomach, small intestine, kidney, cecum, colon, testis, and ovary) (data not illustrated). Female C57BL/6 mice (Janvier, France) or LGP2 TG mice of 6 to 8 weeks of age were inoculated intramuscularly in both hind legs with 1×10^7 infectious particles of RABV. Disease progression was evaluated by scoring clinical signs and mortality as follows: 0 = normal mice, 1 = ruffled fur, 2 = one paralyzed hind leg, 3 = two paralyzed hind legs and hunched back, 4 = tetraplegia (defined as the total loss of mobility), and 5 = death. Data are presented as a cumulative clinical score (the individual clinical score for each mouse was added) and as a mortality curve. In other experiments, groups of mice (n = at least 3) were deeply anesthetized and perfused intracardially with saline phosphate buffer (SPB) with Mg^{2+} and Ca^{2+}. Organs were collected separately and stored at −80°C before being processed for RNA or protein extraction. For immunohistochemistry, mice were perfused with 4% paraformaldehyde in SPB.

Ethical statement. Animal housing and experimental protocols followed guidelines approved by the French Ministry of Agriculture and Institut Pasteur ethical committees. The Institut Pasteur is a member of Le Comité 1 Régional d'Ethique pour l'Expérimentation Animale (CREEA) de l'Ile de France.

Abs and reagents. Antibodies (Abs) were acquired as follows. Rabbit polyclonal anti-LGP2 Ab was from Proteintech Group, Inc., mouse polyclonal anti-tubulin was from Oncogene Research Products, RIG-I-specific mouse monoclonal Ab (MAb) (clone Alme-1) was from Alexis Biochemicals, RIG-I-specific rabbit Ab was from ProSci Inc., fluorescein isothiocyanate (FITC)-conjugated rabbit anti-RABV nucleocapsid Ab was from Bio-Rad, and anti-RABV N protein MAb (PVA-3) was prepared in the laboratory (32). βIII-Tubulin was stained with a mouse MAb (clone 5G8) from Promega. B7-H1 was detected with a rat MAb (clone MIH5) from eBioscience and a rabbit Ab from Santa Cruz, Inc., for immunofluorescence and Western blotting, respectively. An anti-mouse IT-Box-m260 kit from Immuno Tools GmbH was used to phenotype splenocytes and mononuclear cells infiltrating the NS. Glial fibrillary acidic protein (GFAP)-specific Ab (Z 0334) was from Dako, peroxidase polymer-labeled anti-rabbit secondary Ab (Histofine) was from a Simple Stain Mouse Max PO kit (Nicheidi Corporation), and recombinant human IFN-β (Betaferon) was obtained from Schering.

RNA extraction, RT, and qRT-PCR. Total RNAs were extracted with the Qiagen reagent QIAzol and an RNeasy kit (for cells) or a Lipid Tissue Midi kit (for the brain, entire spinal cord, or an equivalent weight of other tissues). RNA quantity and quality were monitored using spectrophotometry (NanoDrop). Reverse transcription-PCR (RT-PCR) was performed using a PX2 thermal cycler with 30 cycles of amplification and 18S rRNA as a reference housekeeping gene. cDNA synthesis was performed from 1 μg RNA, using SuperScript II reverse transcriptase (Invitrogen). Quantitative real-time RT-PCR (qRT-PCR) was performed in duplicate using an ABI Prism 7500 fast sequence detector system with Power SYBR green PCR master mix (Applied Biosystems) or Go *Taq* master mix (Promega). After normalization to 18S rRNA, the relative abundance of mRNA was obtained by calculation of the difference in threshold cycles of the test and control samples (wild-type value = mock value for tissue or noninfected cells [value set to 1]), commonly known as the $\Delta\Delta C_T$ method. RABV RNA quantification was normalized to 18S rRNA and a standard control. Sequences or references for primers used for RT-PCR were published previously (39) or were purchased from Qiagen.

LGP2 overexpression and ISG56 luciferase reporter assay. Cells were transfected with an expression plasmid encoding LGP2 (DHX58; GenBank accession no. NM_024119) under the control of a CAG promoter, using an Amaxa cell line Nucleofector kit V (Lonza). The IFN-stimulated gene 56 (ISG56) luciferase reporter was constructed and assayed as previously described (5). At 12 h post-transfection, cells were infected for 24 h with RABV. Luminescence and absorbance in cell lysates were measured to evaluate luciferase and β-galactosidase expression, respectively. Luminescence levels were normalized to the absorbance level for each sample, and luminescence of RABV-infected samples was expressed relative to that of the noninfected samples.

Western blotting, immunohistochemical staining, and measure of neutralizing antibodies. Western blotting was performed and visualized as previously described (35). For immunohistochemistry, transverse brain sections were embedded in paraffin according to routine protocols and were cut into 5-μm slices. The astrocytes were labeled with primary GFAP Ab (1/300), using a Histofine Simple Stain Mouse Max PO kit. Hematoxylin was used as a counterstain. Positive cells were counted manually in 5 or 6 fields per mouse (magnification, ×100), and means were compared between similar brain sections from WT and LGP2 TG mice. RABV- and mock-infected cells were immunostained and analyzed as previously described (35). The rapid fluorescent-focus inhibition test was used to assay serum samples as previously described (49).

Inflammatory bioarrays. Bioarrays were set up with 100 μg of brain lysate (90 μg/sample), using a mouse inflammation Ab array G series 1 kit from RayBiotech, Inc. Arrays were read on an AxioVision scanner and analyzed using Axon GenePix software. The fluorescence intensity for each spot was normalized to a positive internal control on the array to allow for array comparison. The fluorescence intensity for the WT mock-infected brain was defined as a standard arbitrary value of 100.

Flow cytometry. NS mononuclear cells were collected from homogenates of brain and spinal cord samples onto Percoll gradients as described previously (19). Phenotyping of splenocytes and mononuclear cells infiltrating the NS was performed with appropriate pairs of Abs and assessed by flow cytometry. Data analysis was performed with Cell Quest Pro software.

Statistical analysis. For comparison of groups, Student's t tests were performed, using GraphPad Prism, version 5.00, for Windows. For the animal experiments, collected data were plotted as Kaplan-Meier survival curves.

RESULTS

LGP2 inhibits the *in vitro* RABV-mediated type I IFN response. To test the effect of LGP2 on the RABV-mediated IFN response *in vitro*, we studied the induction of ISG56, one of the most activated genes during RABV infection (39), using an ISG56-dependent luciferase reporter assay on human Hek cells cotransfected with an expression vector carrying human *LGP2* or with a mock plasmid and infected with RABV (Fig. 1A). The effects of LGP2 on the transcription of *IFN*-β and the IFN-inducible gene for 2′,5′-oligoadenylate synthetase 1 (*OAS1*) were also measured by qRT-PCR with LGP2- or mock-transfected cells (Fig. 1B). After a 24-h RABV infection, when LGP2 protein was expressed (Fig. 1A), the luminescence

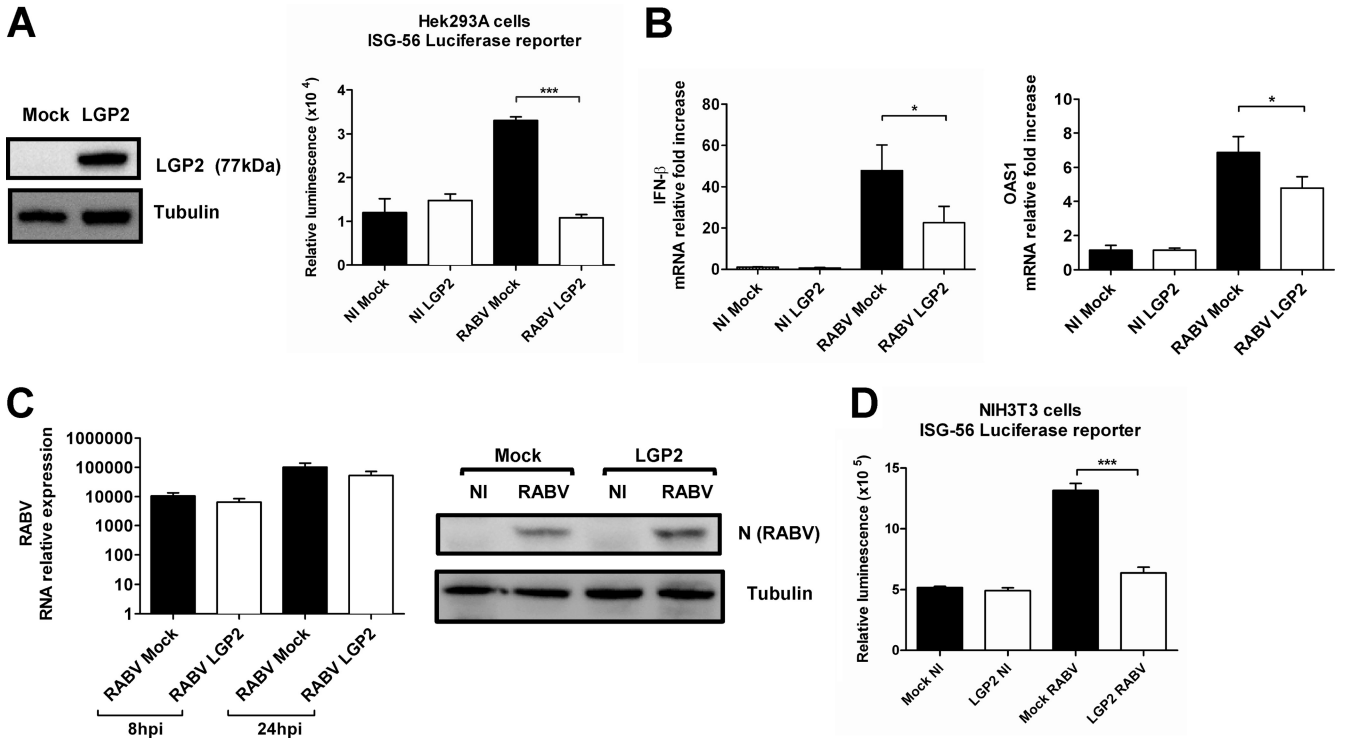

FIG. 1. LGP2 inhibits the type I IFN response during RABV infection *in vitro*. (A) Hek cells were cotransfected with a plasmid encoding a luciferase reporter under the control of an ISG56 promoter, a β-galactosidase-encoding plasmid (used as a transfection efficiency control), and an empty vector (mock) or LGP2-encoding vector (LGP2). LGP2 protein overexpression was checked by Western blotting, with tubulin used as the internal control. After 24 h, luciferase activity was measured by detecting the luminescence in RABV-infected cells ($n = 4$). Data are presented as means and standard errors of the means (SEM) (***, $P \leq 0.0005$). (B) Hek cells transfected with LGP2-encoding vector (LGP2) or an empty vector (mock) were infected with RABV. RNAs were extracted at 24 h p.i., and qRT-PCR targeting *IFN*-β and *OAS1* was performed ($n = 6$). Data are presented as means and SEM (*, $P \leq 0.05$). (C) After 24 h, RABV infection was monitored in LGP2- and empty vector (mock)-transfected cells by qRT-PCR (left) and by Western blotting against the RABV N protein (right). Data are representative of two independent experiments. qRT-PCR results are presented as means and SEM. (D) NIH 3T3 cells were cotransfected as described for panel A. After 24 h, luciferase activity was measured by detecting the luminescence in noninfected (NI) and RABV-infected cells ($n = 4$). Data are presented as means and SEM (***, $P \leq 0.0005$).

activity was two-thirds lower in LGP2-overexpressing cells than in mock-transfected Hek cells (Fig. 1B), and transcription of *IFN*-β and *OAS1* was reduced (Fig. 1B). The lesser induction of *IFN*-β and *OAS1* transcription was not the result of reduced RABV infection in LGP2-transfected cells, because RABV infections in LGP2- and mock-transfected Hek cells did not differ (Fig. 1C). Similar results were obtained when mouse NIH 3T3 fibroblasts were transfected with *LGP2* (Fig. 1D). These data demonstrate that LGP2 functions as an inhibitor of the RABV-triggered IFN-β response *in vitro* in both human and mouse cells, suggesting cross-reactivity of LGP2 in these two mammalian species.

LGP2 protein expression is restricted in WT mouse brain and neuronal cells, even after infection. Because RABV infects the NS, we investigated whether LGP2 is expressed and/or inducible in the NS of the mouse, the animal model for experimental rabies. To characterize LGP2 expression *in vivo*, we compared LGP2 mRNA and protein expression in the hearts, brains, and kidneys of uninfected C57BL/6 mice by qRT-PCR and Western blotting (Fig. 2A). Interestingly, LGP2 protein expression was barely detectable in brain tissue, although mRNAs were present. After an intramuscular injection of RABV, 7 mice were sacrificed at different times postinfection (p.i.) to test for LGP2 induction. RABV transcripts and endogenous mouse LGP2 (mLGP2) mRNAs were measured in brain extracts by qRT-PCR (Fig. 2B). We noticed an increase in LGP2 transcripts that paralleled RABV brain invasion. Nevertheless, LGP2 protein expression in the infected brains remained low or barely detectable by Western blotting, whereas RIG-I protein was easily detected in the same samples. These results indicated that the brain is almost devoid of LGP2 protein, even after RABV infection.

The low expression level of LGP2 in the infected brain might correspond to infiltrated cells or to resident neural cells such as astrocytes (18) or neurons. Because RABV targets mainly neurons, where RABV triggers a RIG-I-mediated innate immune response (22, 39), we further analyzed LGP2 expression in neuronal cells (human postmitotic neurons [NT2N] and human neuroblastoma cells [SKNSH]). RT-PCR with NT2N cells (Fig. 2C, left panel) and qRT-PCR with SKNSH cells (middle panel) revealed increased *LGP2* transcription over a range similar to that for *RIG-I* transcription. Nevertheless, and in contrast to the results with the RIG-I protein, which could be detected in the absence of infection and after infection, LGP2 protein could not be detected under any condition (Fig. 2C, right panel).

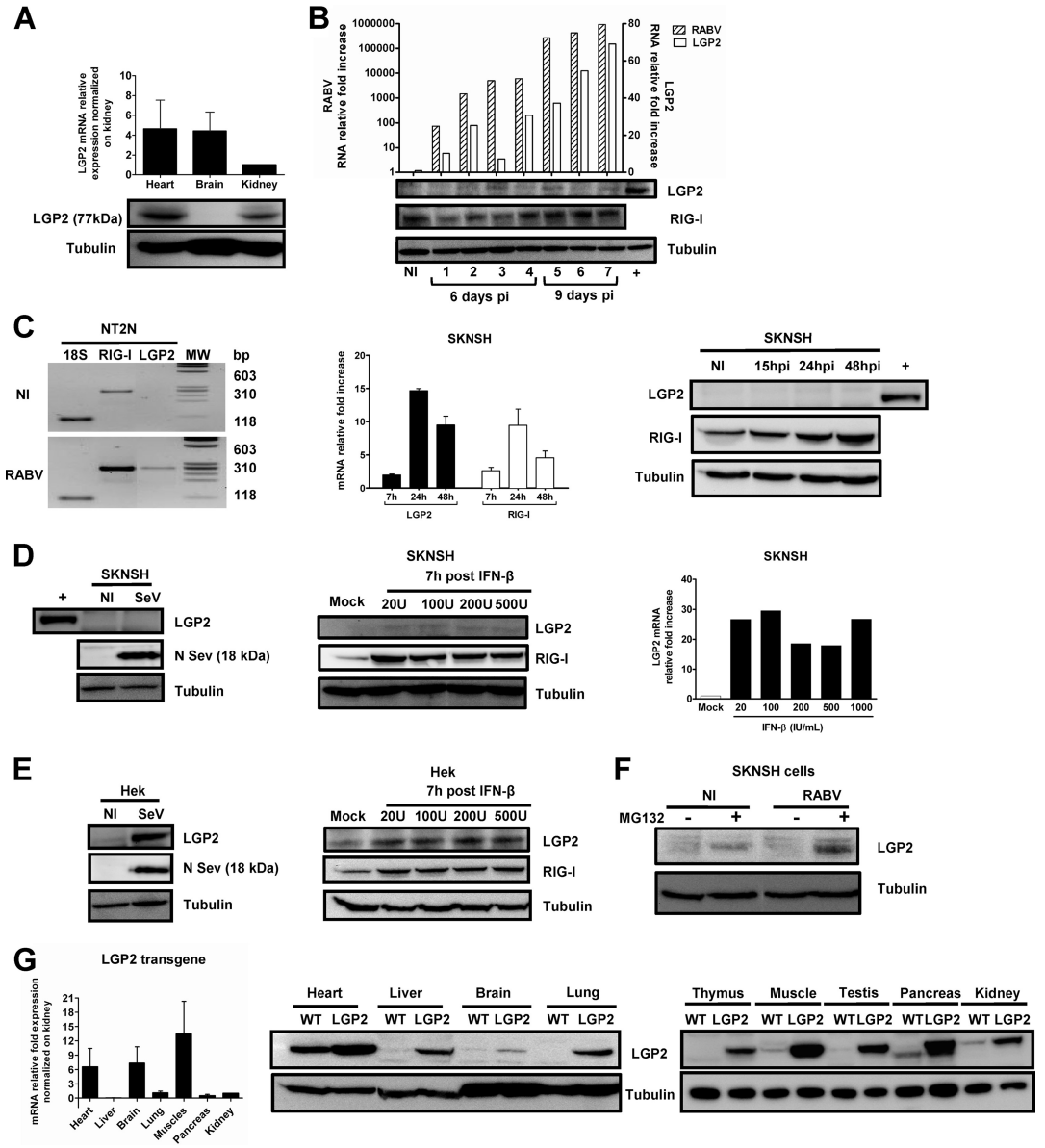

FIG. 2. LGP2 protein expression is strongly restricted in mouse brain and human neuronal cells because of its degradation. (A) *LGP2* mRNA (top) and LGP2 protein (bottom) expression in the hearts, brains, and kidneys of WT mice was quantified by qRT-PCR and normalized to the *LGP2* mRNA level in the kidney (value taken as 1) or determined by Western blotting normalized to tubulin. qRT-PCR data are presented as means and SEM ($n = 4$). (B) Seven RABV-infected mice were sacrificed at different times after virus injection (the first 4 mice were sacrificed at day 6 p.i., and the last 4 were sacrificed at day 9 p.i.). Brains were separated into two parts. One half of the brain was used for qRT-PCR, and the other was used for Western blotting. RABV *N* and endogenous mouse *LGP2* mRNAs in the brains of RABV-infected WT mice or noninfected (NI) animals were quantified by qRT-PCR (top). LGP2, RIG-I (used as a control protein), and tubulin (used as a gel loading control) protein expression in the brains of sacrificed mice was monitored using Western blotting (bottom panels). The positive control (+) is LGP2 expression in a WT heart lysate. (C) *LGP2* and *RIG-I* expression in human postmitotic neurons (NT2N) and neuroblastoma SKNSH cells after RABV infection (24 h for NT2N cells and 7, 15, 24, and 48 h for SKNSH cells) or no infection (NI) was measured by RT-PCR (NT2N cells; 18S rRNA was used as an internal control) and by qRT-PCR (SKNSH cells; values were normalized to the NI control, with a value of 1). Proteins were detected by Western blotting for SKNSH cells, with a heart lysate as a positive control (+) for LGP2 protein ($n = 3$). (D) LGP2 expression in SKNSH cells was measured 24 h after SeV infection by Western blotting (left; SeV N protein expression was used as a control for infection) and 7 h after treatment with increasing doses of IFN-β (20, 100, 200, and 500 IU/ml) by Western blotting (central panel; RIG-I expression was used as a control for IFN-β treatment efficiency) and qRT-PCR (normalized with the mock value, taken as 1). (E) LGP2 expression in nonneuronal cells (Hek) was measured by Western blotting 24 h after SeV infection (left) and 7 h after treatment with increasing IFN-β doses (right). SeV N protein expression was used as a control for infection, RIG-I was used as a control for IFN-β treatment efficacy, and tubulin was used as a control for protein loading. (F) Western blotting showing the effect of MG132 treatment (10 μM) on LGP2 expression in NI and RABV-infected SKNSH cells. (G) LGP2 expression in the brains of LGP2 TG mice. LGP2 protein and *LGP2* mRNA expression was analyzed by qRT-PCR normalized to LGP2 transgenic mRNA levels in the kidney ($n = 4$) (left) (data are presented as means and SEM) and by Western blotting with lysates of hearts, livers, brains, lungs, thymuses, muscles, testes, pancreases, and kidneys of LGP2 TG (LGP2) and WT mice (right). Tubulin was used as a control of protein loading.

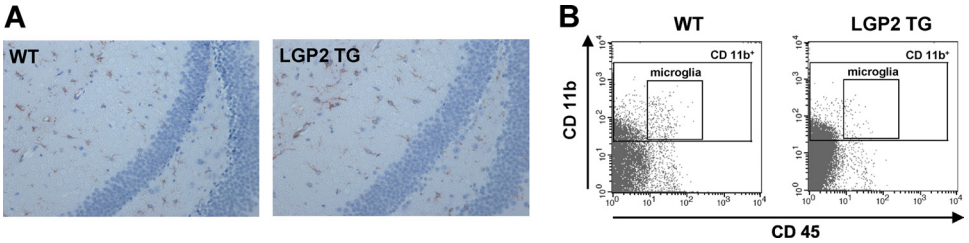

FIG. 3. LGP2 overexpression in LGP2 TG mice does not modify basal gliosis and monocyte influx into the brain. (A) Astrogliosis was assayed by immunohistochemistry on noninfected WT and LGP2 TG paraffin-embedded brain sections, using a GFAP primary Ab. Numbers of $GFAP^+$ cells in the caudal diencephalon were 44.6 ± 4.2 and 51.3 ± 3.1 for WT and LGP2 TG mice, respectively (20 fields were counted per mouse type). (B) Flow cytometry of cells isolated from the NS of WT and LGP2 TG mice by use of a Percoll gradient and double stained with CD11b and CD45 Abs to analyze monocyte infiltration and microglia activation. The $CD11b^+$ cells correspond to infiltrated monocytes (9.7 and 7.5% in WT and LGP2 TG mice, respectively), and the $CD11b^+$ $CD45^{+\ intermediate}$ cells are microglia (1% in both types of mice). Results are representative of two independent experiments.

This absence of LGP2 protein was also observed in SKNSH cells after its induction by either a 24-h SeV infection or a 7-h IFN-β treatment (20 to 1,000 IU/ml) (Fig. 2D), two conditions that result in LGP2 transcription upregulation (26). This indicates that restriction of LGP2 protein expression in neuronal cells is not specific to RABV infection. Furthermore, LGP2 protein expression was observed in cells of nonneuronal origin, such as Hek kidney embryonic cells, after SeV infection or IFN-β treatment, supporting a neuron-specific restriction of LGP2 expression (Fig. 2E). When proteasome activity was inhibited by MG132 treatment, LGP2 protein could be detected in both noninfected and RABV-infected SKNSH cells, suggesting that LGP2 restriction in neuronal cells relies on protein degradation (Fig. 2F). These observations indicated that LGP2 protein expression is naturally restricted in brain and neuronal cells, in particular by cell-specific proteasomal degradation.

LGP2 protein is expressed in the NS of LGP2 TG mice. Despite the natural degradation of LGP2 in the mouse brain, we investigated whether it was possible to force LGP2 expression in the NS by generating a new transgenic mouse model that overexpresses *LGP2* cDNA downstream of the ubiquitous CAG promoter (LGP2 TG mice). Endogenous and transgenic LGP2 expression was measured and compared by qRT-PCR and Western blotting for different organs of WT and LGP2 TG mice (Fig. 2G). For LGP2 TG mice, LGP2 expression was observed in all organs tested. However, despite similar high levels of *LGP2* mRNA in the heart and brain (Fig. 2G, left panel), the brain remained the organ with the lowest level of LGP2 protein (Fig. 2G, middle panel), reflecting the pattern of LGP2 expression already observed in WT mouse organs (Fig. 2A). Nevertheless, LGP2 was present in the mouse brain, making the LGP2 TG mouse a relevant model for studying the role of the RIG-I-mediated innate immune response in the RABV immune response and pathogenesis.

LGP2 overexpression drastically impairs the innate immune response in the NS during RABV infection. Histology analysis performed on brains of noninfected LGP2 TG mice showed no activation of glial cells or enhanced brain immune surveillance (Fig. 3). To test the function of LGP2 in the innate immune response triggered in the NS during RABV infection, WT and LGP2 TG mice were injected intramuscularly in each hind limb with a dose of an encephalitic RABV strain expected to kill 80% of the mice. Brains and spinal cords were sampled 8 and 11 days after injection.

The upregulation of innate immune markers upon RABV infection in the NS of WT mice (transient in spinal cords and sustained in brains, a hallmark of RABV infection) did not occur in the NS of LGP2 TG mice (Fig. 4A). Indeed, after infection, no induction of *IFN*-β, *OAS1*, or *IL-6* was noted compared to that in mock-infected LGP2 TG mice. This absence of upregulation of the innate immune response was also observed at the protein level (Fig. 4B). Indeed, in the brains of WT mice, RABV stimulated the expression of 18 markers of inflammation among the 40 present on the protein array, including chemokines (CCL5, CCL2, CXCL11, and CXCL9), cytokines (interleukin-6 [IL-6], IL-12, and IL-13), and other proteins involved in inflammation (TIMP-1 and -2 and TNFR1). None of these, with the exception of IL-9 and CXCL13, were upregulated by RABV infection in LGP2 TG brains, indicating clearly that the RABV-mediated innate immune response was abrogated in the NS upon LGP2 expression. These data showing that LGP2 overexpression blocks the RABV-induced innate immune response *in vivo* are in agreement with our *in vitro* results (Fig. 1).

LGP2 overexpression reduces RABV morbidity and promotes RABV clearance from the brain. To analyze the effect of the innate immune response impairment on RABV pathogenesis, we compared the progression and outcomes of RABV infection in WT and LGP2 TG mice by recording body weight and clinical signs (ruffled fur, hind-limb paralysis, hunchback [a sign of encephalitis], and death) daily for up to 20 days p.i. As shown in the left panel of Fig. 5A, weight loss appeared at 5 days p.i. and worsened in both groups as the infection progressed. Nevertheless, the weight loss in LGP2 TG mice was significantly less severe than that in WT mice ($P < 0.005$). The cumulative clinical score was significantly decreased in LGP2 TG mice compared to that in WT mice between days 7 and 12 p.i. (Fig. 5A, middle panel). Indeed, the mean delay between the first sign of hunchback and death was significantly greater in LGP2 TG mice than in WT mice (2.8 and 1.6 days, respectively; $P < 0.05$). However, despite the slower disease progression in LGP2 TG mice, the mortality of LGP2 TG mice did not differ significantly from that of WT mice (day 20 mortality, 62% and 75%, respectively) (Fig. 5A, right panel).

RABV neuroinvasiveness was monitored in the spinal cords

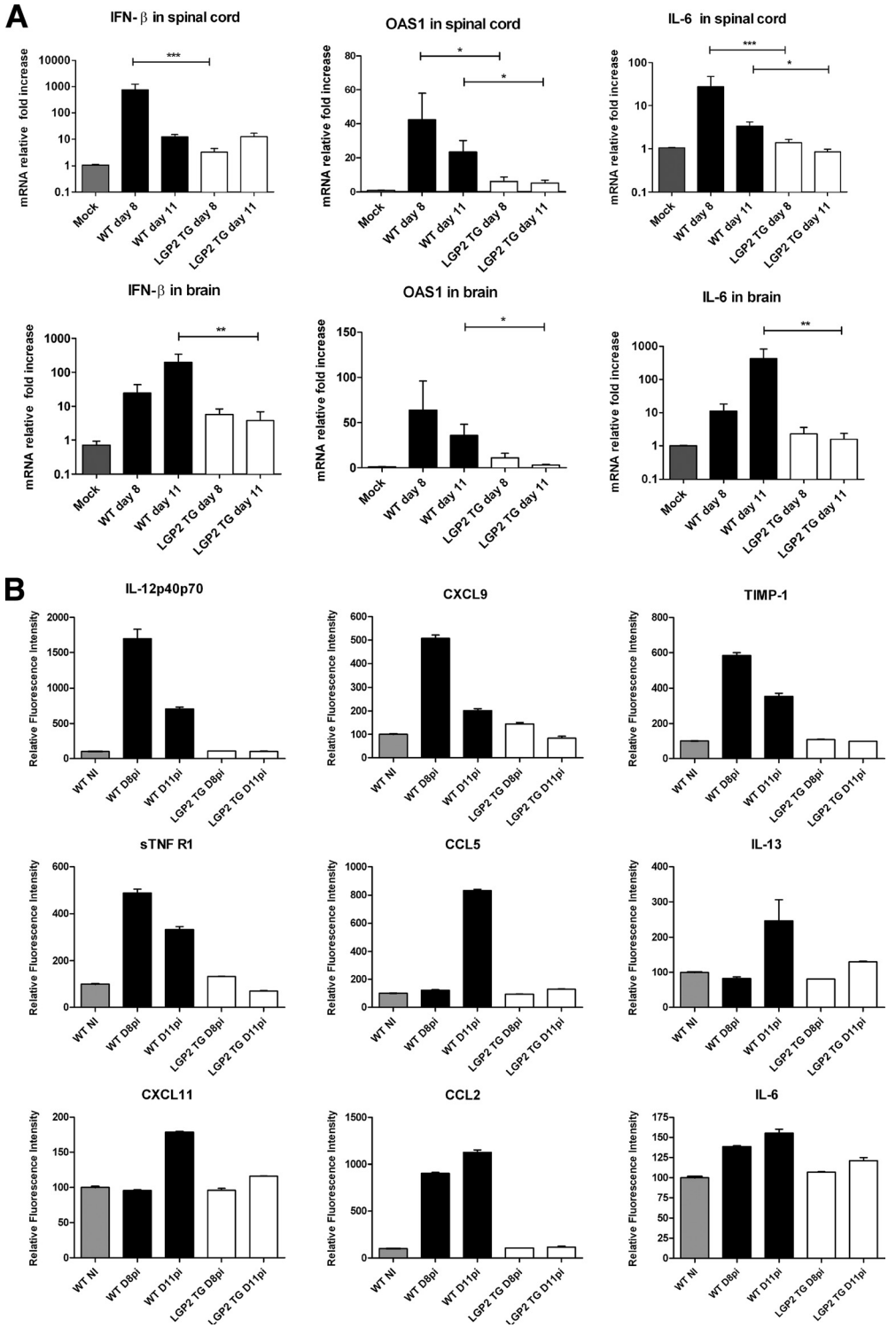

FIG. 4. LGP2 inhibits RABV-triggered type 1 IFN and inflammatory responses in the infected NS. (A) *IFN*-β, *OAS1*, and *IL-6* transcripts in the spinal cords (upper row) and brains (lower row) of WT and LGP2 TG mice sacrificed on day 8 and day 11 p.i. ($n = 7$ or 8) were quantified by qRT-PCR and normalized to values obtained for mock-infected tissues (value set to 1). Data are presented as means and SEM (*, $P \leq 0.05$; **, $P \leq 0.005$; ***, $P \leq 0.0005$). (B) Inflammatory bioarray analysis of markers of IFN-mediated and inflammatory responses (IL-12p40p70, CXCL9, TIMP-1, sTNF-R1, CCL5, IL-13, CXCL11, CCL2, and IL-6) in NI and RABV-infected brains of WT and LGP2 TG mice at days 8 and 11 p.i. ($n = 2$) (normalized value = 100 for NI WT mouse brain). The results are representative of two independent experiments.

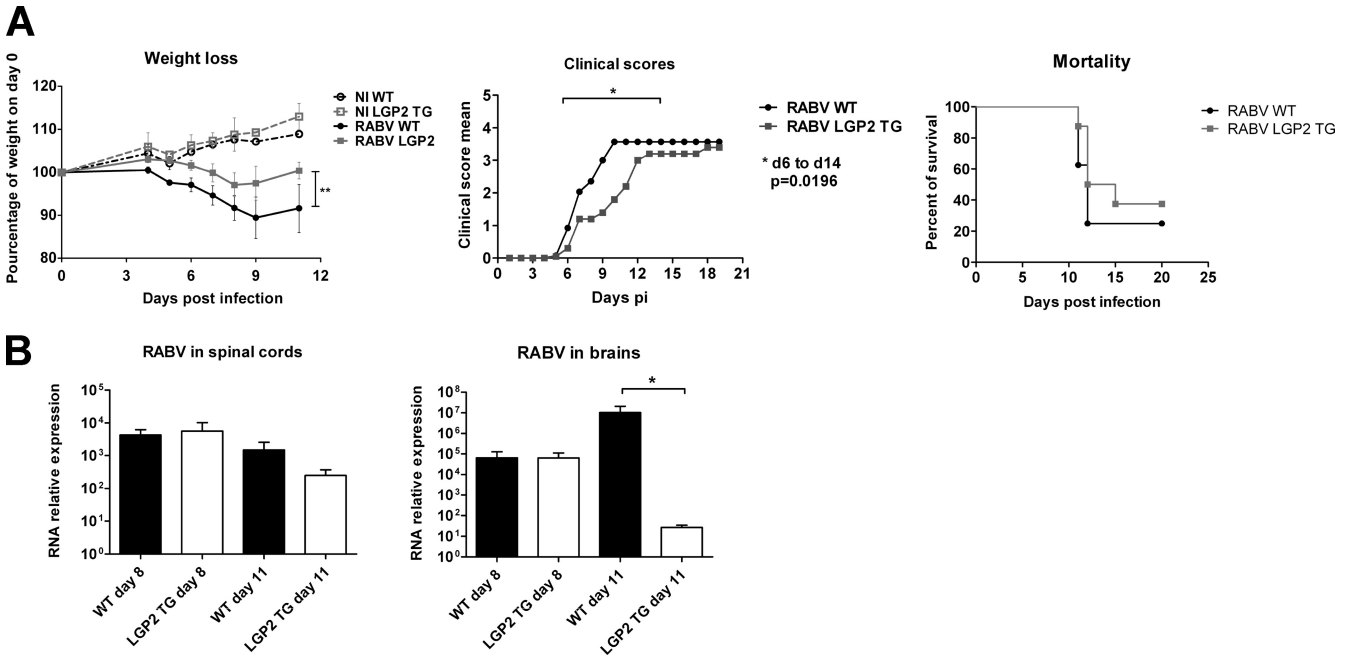

FIG. 5. Forced expression of LGP2 slows down RABV clinical progression and favors RABV clearance from the brain. WT and LGP2 TG mice ($n = 8$) were injected intramuscularly with a dose of an encephalitic strain of RABV sufficient to kill 80% of injected mice. (A) Clinical signs of rabies (body weight loss, cumulative clinical scores) and mortality curves were followed in WT (black) and LGP2 TG (gray) mice. Results are representative of at least three independent experiments. (B) RABV neuroinvasiveness in the spinal cords and brains of WT and LGP2 TG mice was compared by qRT-PCR targeting the RABV N protein at 8 and 11 days p.i. ($n = 7$ or 8). Data are presented as means and SEM (*, $P \leq 0.05$).

and brains of RABV-infected WT and LGP2 TG mice by measurement of the amount of N viral gene transcripts (Fig. 5B). Viral transcription in the spinal cord was similar between the two groups at days 8 and 11 p.i., whereas it was drastically reduced in the brains of LGP2 TG mice at day 11 p.i. (10^7-fold less than in the brains of WT mice) (Fig. 5B, right panel). In addition, the kinetics of brain invasion indicated that in contrast to WT mice, the LGP2 TG mice had almost cleared the infection from the brain at day 11 p.i. Nevertheless, this clearance was not sufficient to protect the mice from a fatal outcome. In conclusion, LGP2 overexpression, which blocks the innate immune response induced by RABV in the NS, does not modify disease outcome; nevertheless, it favors viral clearance from the LGP2 TG brain and allows significantly reduced signs of disease.

LGP2 overexpression does not modify humoral response and T cell phenotypes in the periphery. To study the origin of this viral clearance, we hypothesized that the immune response in the periphery could be more efficient in LGP2 TG mice than in WT mice. Specific emphasis was given to the humoral response because RABV-specific neutralizing Abs play a crucial role in protection against RABV infection (10). However, the neutralizing Ab reached similar titers in the blood of WT and LGP2 TG mice (Fig. 6A). In addition, the phenotypes of immune cells in the spleens of RABV-infected WT and LGP2 TG mice (at days 5 and 8 p.i.) were not significantly different, showing similar CD4/CD8 ratios and similar proportions of B cells (Fig. 6B, left and right panels, respectively). These observations suggest that LGP2 overexpression does not cause a major effect on the setting up of the immune response in the periphery during RABV infection.

LGP2 overexpression slows down leukocyte infiltration into the NS and limits destruction of infiltrated CD8$^+$ T cells. Because activated microglia and infiltrated leukocytes in the inflammatory brain can contribute to viral clearance (46), we compared the activation of microglia and the numbers of infiltrated leukocytes in the NS of LGP2 TG and WT mice (Fig. 7A).

Percentages of monocytes (CD11b$^+$ cells), microglias (CD11b$^+$ CD45$^{+\ \text{intermediate}}$), and activated microglias/macrophages (CD11b$^+$ CD45$^{+\ \text{high}}$) were identical at 6 days p.i. in both groups of mice (Fig. 7A), suggesting that RABV clearance in LGP2 TG mice does not result from higher microglia activation. No difference was seen in B cell infiltration (Fig. 7B). In contrast, the numbers of T cells (T cell receptor α/β positive [TCRα/β^+]) and CD4$^+$ T cells were lower in LGP2 TG mouse brains than in WT brains at 6 days p.i. (Fig. 7C and D). This decline in T cells is consistent with the smaller inflammatory and chemoattractive response observed in RABV-infected LGP2 TG NS than in WT NS (Fig. 4).

Since T cell-mediated IFN-γ-dependent inflammation has been identified as a factor clearing RABV infection from the NS (19, 21), we analyzed whether IFN-γ expression was different in the NS of LGP2 TG mice and WT mice. As shown in Fig. 7E, RABV infection upregulated IFN-γ expression to similar ranges in both WT and LGP2 TG mouse brains (similar data were obtained for spinal cords). These data indicate that higher IFN-γ expression is not responsible for better viral clearance in the LGP2 TG mouse brain.

Because RABV has evolved an immunoevasive strategy mainly through the destruction/exhaustion of infiltrated CD8$^+$ T cells in the NS (1, 28), we studied whether the innate im-

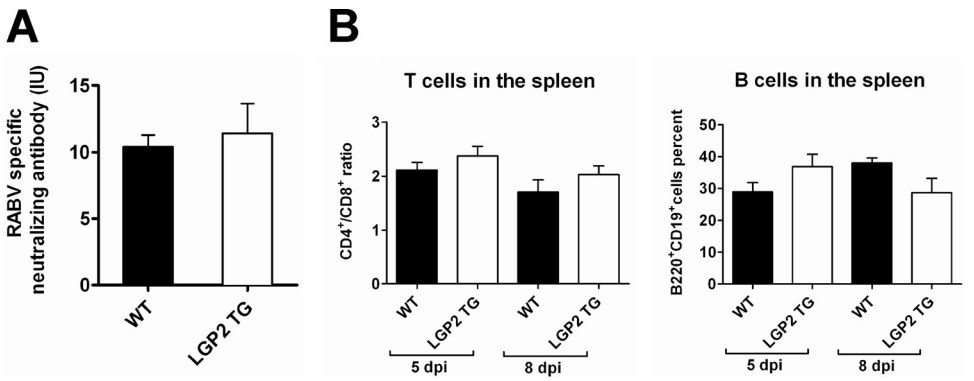

FIG. 6. Innate immune impairment does not modify immune parameters in the periphery. (A) RABV-specific neutralizing Ab titers (expressed in international units per ml [IU/ml]) in the blood were compared by the rapid fluorescent-focus inhibition technique, using WT and LGP2 TG mouse sera taken at 11 days p.i. ($n = 9$ and 8, respectively). (B) LGP2 TG and WT mice exhibited similar spleen subpopulations. Spleen cells of RABV-infected WT and LGP2 TG mice ($n = 4$) were taken at days 5 and 8 p.i. and stained with paired Abs for CD4 and CD8 or B220 and CD19. Percentages of $CD4^+$ $CD8^+$ and $CD19^+$ $B220^+$ cell populations were analyzed by flow cytometry. Results are presented as $CD4^+/CD8^+$ ratios and percentages of $B220^+$ $CD19^+$ cells ($n = 8$).

mune response impairment in LGP2 TG mice affects $CD8^+$ T cell elimination and thus may explain RABV clearance in the transgenic mouse brain. For this purpose, we compared the fate of $CD8^+$ T cells in the NS of RABV-infected LGP2 TG and WT mice (Fig. 7F and G). Six days after infection, similar amounts of $CD8^+$ T cells were observed in the brain infiltrates of RABV-infected LGP2 TG and WT mice (Fig. 7F, left panel). However, the $CD8^+$ T cell proportion dropped from 35% to 12% in WT mouse brains between day 5 and day 8 p.i., whereas this population decreased from 43% to 24% in the infected LGP2 TG mouse brains (Fig. 7F, middle panels). Thus, the drop of $CD8^+$ T cells among $CD3^+$ T cells that occurred between day 5 and day 8 in the RABV-infected brains was smaller in LGP2 TG mice (−41%) than in WT mice (−68%) (Fig. 7F, right panel).

Similarly, when 6-day RABV-infected WT and LGP2 TG mice were sorted according to the severity of clinical signs (group 1, weight loss of <5%; and group 2, weight loss of >5%) (Fig. 7G), the expected drop among migratory $CD8^+$ T cells caused by RABV was observed between groups 1 and 2 of WT mice and not between the LGP2 TG groups. These data indicate that LGP2 overexpression is associated with protection of the migratory $CD8^+$ T cells in the NS.

Altogether, these results indicate that the impairment of the innate immune response in the RABV-infected NS of LGP2 TG mice reduces the infiltration of immune migratory cells but keeps IFN-γ expression constant and specifically protects the subpopulation of infiltrated $CD8^+$ T cells.

LGP2 overexpression impairs B7-H1 induction in RABV-infected NS and primary neurons. In the RABV-infected WT brain, the drop in migratory $CD8^+$ T cells can result in the upregulation of B7-H1 protein in the NS (28). Indeed, the expression of the IFN-inducible B7-H1 protein contributes to the exhaustion (16) or destruction (13) of $CD8^+$ T cells that are potentially responsible for RABV clearance (19). In this context, it is expected that a lower level of *B7-H1* expression would be associated with reduced RABV neuroinvasiveness. We therefore compared B7-H1 expression (mRNA and protein) in the NS of RABV-infected LGP2 TG and WT mice (Fig. 8A and B). The RABV-mediated upregulation of *B7-H1* mRNA observed in WT brains at days 8 and 11 p.i. was significantly reduced in LGP2 TG brains (10-fold less in LGP2 TG mouse brains) (Fig. 8A). Similarly, the RABV-mediated upregulation of B7-H1 protein observed in WT brains at day 8 or 11 p.i. was not observed in RABV-infected LGP2 TG mouse brains (Fig. 8B).

We also performed immunocytochemistry of B7-H1 protein expression in primary neuronal cultures prepared from dorsal root ganglia of adult spinal cords of WT and LGP2 TG mice after *in vitro* RABV infection (Fig. 8C). In contrast to neurons obtained from WT mice, in which RABV infection triggered strong B7-H1 protein expression, neurons obtained from LGP2 TG mice, despite an equal level of infection, showed only weak expression of B7-H1 protein upon infection.

These data indicate that LGP2 overexpression decreases neuronal B7-H1 expression, a feature consistent with protection of migratory $CD8^+$ T cells and with viral clearance from the LGP2 TG mouse brain.

DISCUSSION

In this study, we observed that LGP2 expression is tightly regulated and not ubiquitous, as previously suggested (11, 17, 30). Remarkably, in the absence of infection, neurons and microglia express low levels of LGP2 protein, if they express any, with the exception of *ex vivo* primary astrocytes in cultures (11, 17). In the LGP2 TG mouse, LGP2 protein expression reached the lowest level in the brain compared with other tissues, despite similar LGP2 transcription levels. Results with MG132 treatment suggest that LGP2 is actively degraded in neuronal cells and thus cannot exert its inhibitory function in this tissue. Lech and colleagues (30) observed that the RIG-I-like helicase distribution varies drastically among tissues, suggesting that knowledge of the RIG-I-like helicase distribution is crucial in the design of experiments. This supports the suitable choice of LGP2 overexpression rather than the use of mice lacking LGP2 ($LGP2^{-/-}$ mice) to modulate the innate immune response and address its function in the course of a strictly neurotropic virus infection.

We showed that LGP2 functions as an inhibitor of the innate

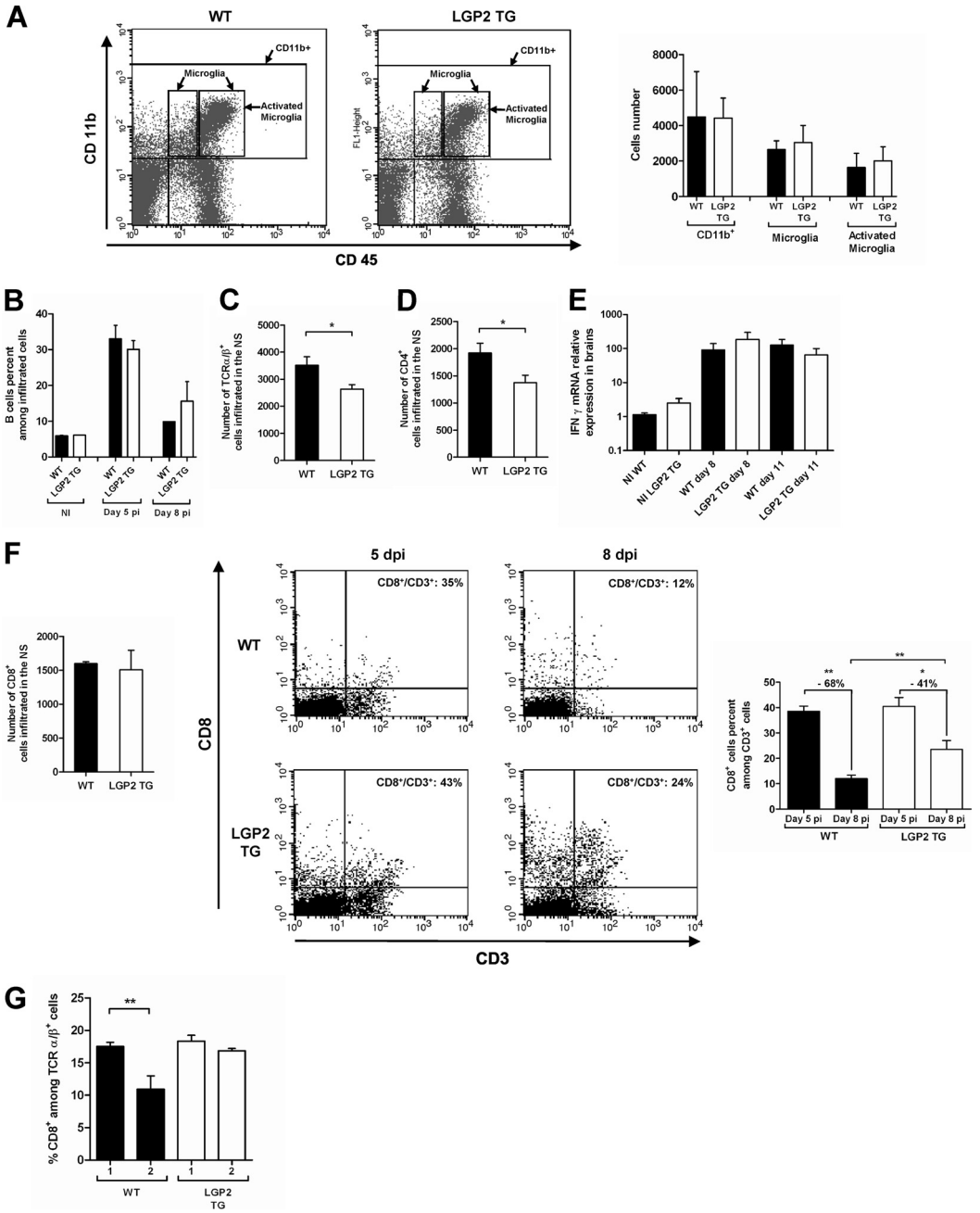

FIG. 7. Innate immune impairment does not modify activation of microglia or IFN-γ mRNA expression but inhibits T cell infiltration and prevents $CD8^+$ T cell destruction in RABV-infected brains. (A) Microglia activation was analyzed by flow cytometry with cells isolated from the NS of day 6 RABV-infected WT and LGP2 TG mice by use of a Percoll gradient and double stained with CD11b and CD45 Abs. Results are representative of two independent experiments. The numbers of monocytes ($CD11b^+$ cells), microglia cells/macrophages ($CD11b^+$ $CD45^+$ [intermediate and high]), and activated microglia cells/macrophages ($CD11b^{+\,high}$ $CD45^+$) in the infiltrates of 6 day RABV-infected WT and LGP2 TG mice ($n = 6$) were compared. (B) Kinetics of infiltrated B cells ($B220^+$ $CD19^+$) in NI and day 5 and day 8 RABV-infected WT and LGP2 TG mice ($n = 6$) were compared. (C) T cell ($TCR\alpha/\beta^+$) infiltration of the NS in the two types of mice was compared at 6 days p.i. ($n = 6$). Data are presented as means for total infiltrated cells, with SEM. *, $P < 0.05$. (D) $CD4^+$ T cell infiltration into the day 6 infected NS of WT and LGP2 TG mice was compared. *, $P < 0.05$. (E) *IFN*-γ transcripts in the brains of WT and LGP2 TG mice sacrificed at day 8 and day 11 p.i. ($n = 7$ or 8) were quantified by qRT-PCR and normalized to values obtained for NI tissues (set to 1). Data are presented as means and SEM. (F) Comparison of $CD8^+$ T cell infiltration in the NS of RABV-infected WT and LGP2 TG mice. (Left) $CD8^+$ T cell infiltration in the infected NS of WT and LGP2 TG mice was compared at 6 days p.i. (Middle) Flow cytometry diagrams of CD8 and CD3 double-stained cells isolated from the NS of WT and LGP2 TG mice at 5 and 8 days p.i. Numbers in the top right quadrants correspond to the percentage of $CD8^+$ T cells among $CD3^+$ T cells ($CD8^+/CD3^+$). (Right) Drops in $CD8^+$ T cells between day 5 and day 8 in WT and LGP2 TG mice ($n = 6$) were compared. *, $P < 0.05$; **, $P < 0.005$. (G) Flow cytometry analysis of cells isolated from the NS of WT and LGP2 TG mice and double stained with CD8 and TCRα/β or CD8 and CD3 Abs. Percentages of $CD8^+$ T cells among $TCR\alpha/\beta^+$ T cells in the NS of two groups each (1 and 2) of WT and LGP2 TG mice were compared at day 6 p.i. Groups 1 and 2 were determined according to the severity of clinical signs, as follows: group 1, weight loss of <5% of initial body weight, with mild clinical signs; and group 2, weight loss of >5% of initial body weight, with severe clinical signs ($n = 4$ in each group). Data are presented as mean percentages of $CD8^+$ T cells among $TCR\alpha/\beta^+$ T cells, with SEM. **, $P \leq 0.005$.

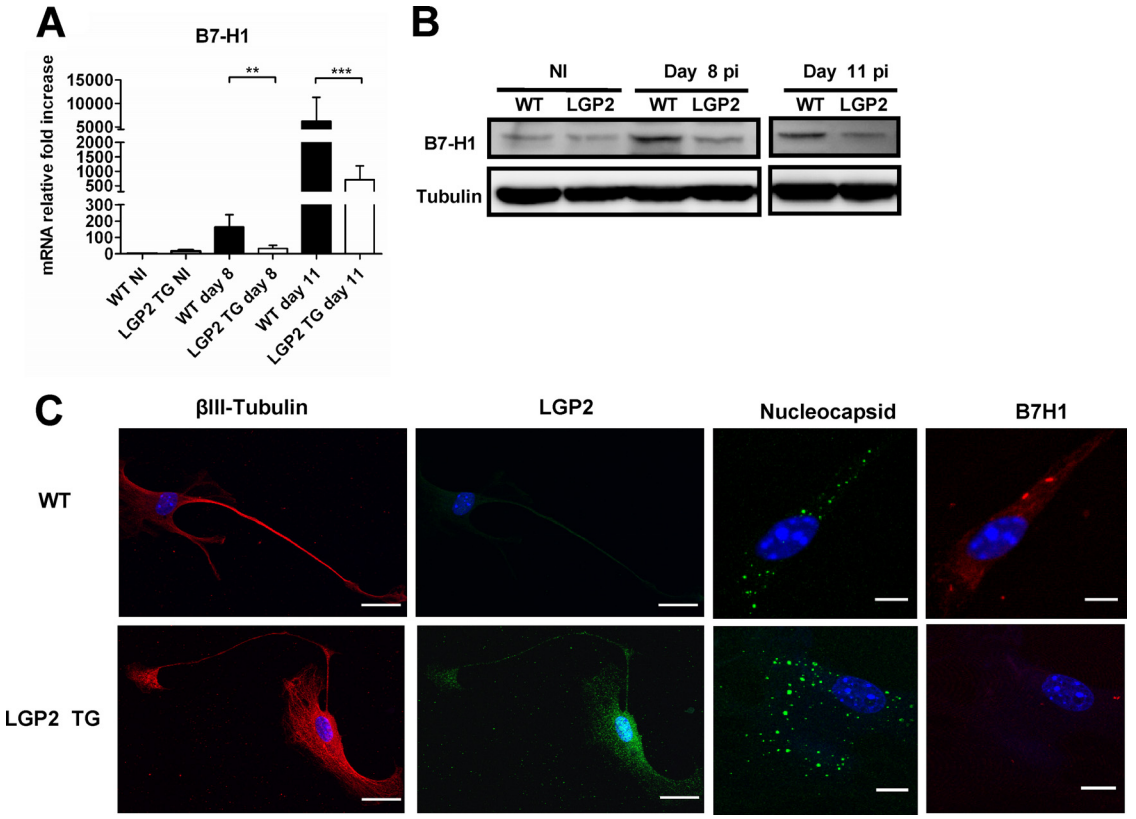

FIG. 8. LGP2 inhibits RABV-induced B7-H1 expression in both NS and dorsal root ganglion neurons. B7-H1 expression in WT and LGP2 TG brains was measured by qRT-PCR ($n = 7$ or 8) (A) or by Western blotting (B) in the absence of infection (NI) or at 8 and 11 days p.i. Data are presented as means and SEM (**, $P \leq 0.005$; ***, $P \leq 0.0005$). (C) Primary neurons from dorsal root ganglia of adult WT (upper row) and LGP2 TG (lower row) mice were infected with RABV. Neurons were immunostained with paired Abs directed against βIII-tubulin (a marker for neurons), LGP2, RABV nucleocapsid, or B7-H1. The percentages of infected cells were similar (58.5% and 62.0% of RABV-infected cells) for WT and LGP2 TG cultures. Bar, 10 μm.

immune response triggered by RABV infection. Evidence of the inhibitory function of LGP2 in the type I IFN response during RABV infection was obtained both *in vivo* and *in vitro* in different cell types. ISG56 expression was reduced in LGP2-transfected mouse and human fibroblasts (Hek), and LGP2-transfected Hek cells had reduced IFN-β and IFN-related gene expression compared to mock-transfected cells. Moreover, cultures of primary neurons from LGP2 TG mice showed reduced expression of the IFN-regulated protein B7-H1. These results are in agreement with the inhibitory role of LGP2 previously observed after VSV infection of LGP2$^{-/-}$ mouse embryonic fibroblasts and macrophages (54). In contrast, they are in contradiction with a report describing LGP2 as a positive regulator of the RIG-I pathway in conventional dendritic cells (cDCs) from LGP2$^{-/-}$ mice infected with VSV (47). This finding may suggest that LGP2 is a positive regulator specifically in cDCs but not in other cell types (47, 54). In this case, the cell type could determine the inhibitory or positive regulatory function of LGP2. Further studies, such as those comparing the properties of DCs isolated from WT and LGP2 TG mice, will be required to address this point more directly.

Concerning RABV infection, a recent study demonstrated that DC activation after exposure to RABV is dependent on type I IFN receptor signaling rather than on RIG-I signaling (15). The fact that activation of DCs in the periphery relies on a signaling pathway independent of LGP2 regulation may explain why the production of RABV-specific neutralizing antibodies and the phenotype of spleen immune cells did not differ between WT and LGP2 TG mice. These results suggest that the LGP2 TG mouse phenotype during RABV infection is driven mostly by the function of LGP2 in the NS.

After RABV infection, the LGP2 TG mice exhibited fewer clinical signs. The overexpression of LGP2 and the associated impairment of the innate immune response resulted in a delay in morbidity (ruffled fur, weight loss, hind-limb weakness, and paralysis), suggesting that RABV morbidity results from an immunopathological mechanism. RABV infection, in contrast to that with other encephalitic viruses, such as West Nile virus (4, 51), is characterized by a modest inflammatory response in the NS (27). Nevertheless, some cytokines, such as IL-6 or IL-12, known to be the main culprits of immunopathology in other diseases (43), are expressed in the RABV-infected NS. The overexpression of LGP2 was accompanied by a reduced expression of IL-6 and a downregulation of the chemokines CCL9 and CXCL11. In their absence, CD4$^+$ T cell infiltration into the RABV-infected NS was reduced. Since migratory T cells have been shown to also participate in RABV morbidity (19, 21, 59), both the limited inflammation and infiltration

contribute to the reduction of RABV morbidity in LGP2 TG mice. Our study confirms the contribution of innate immunity to morbidity during neurotropic viral infections (57) and demonstrates that the RIG-I-mediated innate immune response participates in RABV morbidity. Such a finding is not totally unexpected, because the contribution of the innate immune response to morbidity has already been observed with other neurotropic viral infections (57). However, it was surprising that LGP2 TG mice, in which the innate immune response, including the type I IFN response, is impaired, did not show more but less infection of the brain. The type I IFN response has been shown to exert antiviral functions in several viral infections. Along this line, the lesser type I IFN response in the NS of LGP2 TG mice should have resulted in a higher infection level of the LGP2 TG mouse NS than that in WT mice. However, this was not the case, since after the peripheral viral injection the spinal cords were equally infected in the two types of mice. This observation, together with previous studies investigating the role of IFN in rabies (28, 33, 36), questions the efficiency of IFN in controlling RABV infection in the NS. In the same vein, since several studies have pointed out that infiltrating T cells recruited into the brain by chemokines have a direct antiviral effect on RABV infection (14, 19, 59), it was expected that mice exhibiting reduced T cell infiltration, as LGP2 TG mice do, would be less able to control RABV spread in the NS than WT mice. In striking contrast, LGP2 TG mice, not WT mice, eliminated RABV infection from the brain at day 11 p.i. This discrepancy suggests that factors other than the size of the infiltrates of immune effectors in the brain may contribute to viral clearance. In the RABV-infected NS, infiltrated T cells have been shown to express several markers of activation, including IFN-γ (19). The fact that IFN-γ expression was similar in the NS of LGP2 TG and WT mice, despite a reduction in the pool of migratory T cells, suggests that the activation of the infiltrated T cells could be stronger in LGP2 TG mice than in WT mice.

Since RABV has evolved an immunoevasive strategy founded on the destruction/exhaustion of infiltrated $CD8^+$ T cells in the NS of infected mice (1, 28), we analyzed whether the drop of $CD8^+$ T cells, a hallmark of RABV infection in the NS of WT mice, was interrupted in LGP2 TG mice. We observed that the disappearance of $CD8^+$ T cells was indeed decreased in the NS of RABV-infected LGP2 TG mice compared to that in WT mice. Because we have previously shown that in the absence of B7-H1 expression, the pool of migratory $CD8^+$ T cells is preserved and RABV infection in the brain is controlled (28), it was tempting to check whether the expression of this immunoevasive protein was decreased in LGP2 TG mice. Indeed, the $CD8^+$ T cell persistence in LGP2 TG mice was concomitant with reduced expression of the IFN-inducible B7-H1 protein. Here we showed that neurons were costained with B7-H1 in DRG cultures. Tumor cells, dendritic cells, neurons, and astrocytes are the cells most commonly expressing B7-H1, but T cells can also express B7-H1 under certain conditions (12, 28, 48). A previous study showed no evidence that infiltrated $CD3^+$ T cells expressed B7-H1 in the RABV-infected brain (28). We cannot completely exclude the possibility that some T cells contribute to B7-H1 expression in the NS of infected mice, but this contribution should be modest. Thus, we propose that B7-H1 downregulation in neural cells probably relies on a type I IFN-dependent mechanism.

These data indicate that innate immune impairment correlates with a decrease of T cell infiltration, B7-H1 induction, and a preservation of activated $CD8^+$ T cells in the LGP2 TG mouse brain. Altogether, these mechanisms might explain the RABV clearance in the brain seen in LGP2 TG mice.

Despite virus clearance, the mortality of LGP2 TG mice was not different from that of WT mice, suggesting that the compensatory mechanism resulting in protection of the $CD8^+$ T cells discussed above is insufficient to counterbalance the lower T cell infiltration and to avoid death. In a previous study, when B7-$H1^{-/-}$ mice were infected with RABV, mortality was drastically reduced and the severity of RABV pathogenesis was inversely correlated with the number of $CD8^+$ T cells in the NS (28). This apparent discrepancy concerning the role of RABV immunoevasion in disease outcome may be explained by the lower T cell infiltration into the LGP2 TG NS than into that of WT mice. This lower T cell infiltration probably leads to less efficient RABV elimination in LGP2 TG mice than that in B7-$H1^{-/-}$ mice. The exact mechanisms causing death in rabies are not well understood, and some may be related to neuronal exhaustion and hormonal deregulation resulting in a lethal "stress" (53). A delay in viral clearance such as that observed in LGP2 TG mice may result in exposure to RABV-mediated "stress" for long enough to cause host death.

Altogether, our results suggest that RABV circumvents the host IFN response to only a limited extent and that the escaped amount of IFN is sufficient to stimulate B7-H1 expression. Thus, we surmise that the efficiency of RABV immunoevasion relies, paradoxically, on the protective mechanism triggered by the host to fight the infection. In this line, it is tempting to propose that the absence of LGP2 in the NS could be a factor that also favors completion of the life cycle of this neurotropic virus.

ACKNOWLEDGMENTS

We are grateful to Christophe Préhaud and Henri Buc for helpful advice; to Eliane Meurs, Stephanie Dabo, and Damien Vitour, Unité Immunité des Hepacivirus, Institut Pasteur, for helpful discussions and for supplying reagents; to Viviane Balloy, Unité de Défense Innée et Inflammation, headed by Michel Chignard at the Institut Pasteur, for breeding the LGP2 mice; to Dominique Come, Unité de Recherche et d'Expertise en Histotechnologie et Pathologie, Institut Pasteur, for skillful help with immunohistochemistry experiments; and to Odile Sismeiro from the Puces à ADN Core Facility, Institut Pasteur, for kind help with the AxioVision scanner.

This work was supported by internal grants from the Institut Pasteur, including PTR 186. Damien Chopy is the recipient of a fellowship from the French Ministère de l'Enseignement Supérieur et de la Recherche.

REFERENCES

1. **Baloul, L., S. Camelo, and M. Lafon.** 2004. Up-regulation of Fas ligand (FasL) in the central nervous system: a mechanism of immune evasion by rabies virus. J. Neurovirol. **10:**372–382.
2. **Bamming, D., and C. M. Horvath.** 2009. Regulation of signal transduction by enzymatically inactive antiviral RNA helicase proteins MDA5, RIG-I, and LGP2. J. Biol. Chem. **284:**9700–9712.
3. **Blondel, D., et al.** 2002. Rabies virus P and small P products interact directly with PML and reorganize PML nuclear bodies. Oncogene **21:**7957–7970.
4. **Brehin, A.-C., et al.** 2008. Dynamics of immune cell recruitment during West Nile encephalitis and identification of a new CD19+ B220− BST-2+ leukocyte population. J. Immunol. **180:**6760–6767.
5. **Breiman, A., et al.** 2005. Inhibition of RIG-I-dependent signaling to the

interferon pathway during hepatitis C virus expression and restoration of signaling by IKKepsilon. J. Virol. **79:**3969–3978.
6. **Camelo, S., M. Lafage, A. Galelli, and M. Lafon.** 2001. Selective role for the p55 Kd TNF-alpha receptor in immune unresponsiveness induced by an acute viral encephalitis. J. Neuroimmunol. **113:**95–108.
7. **Camelo, S., M. Lafage, and M. Lafon.** 2000. Absence of the p55 Kd TNF-alpha receptor promotes survival in rabies virus acute encephalitis. J. Neurovirol. **6:**507–518.
8. **Castellanos, J. E., et al.** 2005. Studying neurotrophin antiviral effect on rabies-infected dorsal root ganglia cultures. J. Neurovirol. **11:**403–410.
9. **Chelbi-Alix, M. K., A. Vidy, J. El Bougrini, and D. Blondel.** 2006. Rabies viral mechanisms to escape the IFN system: the viral protein P interferes with IRF-3, Stat1, and PML nuclear bodies. J. Interferon Cytokine Res. **26:**271–280.
10. **Cox, J. H., B. Dietzschold, and L. G. Schneider.** 1977. Rabies virus glycoprotein. II. Biological and serological characterization. Infect. Immun. **16:**754–759.
11. **Cui, S., et al.** 2008. The C-terminal regulatory domain is the RNA 5′-triphosphate sensor of RIG-I. Mol. Cell **29:**169–179.
12. **Dong, H., and L. Chen.** 2003. B7-H1 pathway and its role in the evasion of tumor immunity. J. Mol. Med. **81:**281–287.
13. **Dong, H., et al.** 2002. Tumor-associated B7-H1 promotes T-cell apoptosis: a potential mechanism of immune evasion. Nat. Med. **8:**793–800.
14. **Fabis, M. J., T. W. Phares, R. B. Kean, H. Koprowski, and D. C. Hooper.** 2008. Blood-brain barrier changes and cell invasion differ between therapeutic immune clearance of neurotrophic virus and CNS autoimmunity. Proc. Natl. Acad. Sci. U. S. A. **105:**15511–15516.
15. **Faul, E. J., et al.** 2010. Rabies virus infection induces type I interferon production in an IPS-1 dependent manner while dendritic cell activation relies on IFNAR signaling. PLoS Pathog. **6:**e1001016.
16. **Freeman, G. J., et al.** 2000. Engagement of the PD-1 immunoinhibitory receptor by a novel B7 family member leads to negative regulation of lymphocyte activation. J. Exp. Med. **192:**1027–1034.
17. **Furr, S. R., V. S. Chauhan, D. Sterka, Jr., V. Grdzelishvili, and I. Marriott.** 2008. Characterization of retinoic acid-inducible gene-I expression in primary murine glia following exposure to vesicular stomatitis virus. J. Neurovirol. **14:**503–513.
18. **Furr, S. R., M. Moerdyk-Schauwecker, V. Z. Grdzelishvili, and I. Marriott.** 2010. RIG-I mediates nonsegmented negative-sense RNA virus-induced inflammatory immune responses of primary human astrocytes. Glia **58:**1620–1629.
19. **Galelli, A., L. Baloul, and M. Lafon.** 2000. Abortive rabies virus central nervous infection is controlled by T lymphocyte local recruitment and induction of apoptosis. J. Neurovirol. **6:**359–372.
20. **Greenwald, R. J., G. J. Freeman, and A. H. Sharpe.** 2005. The B7 family revisited. Annu. Rev. Immunol. **23:**515–548.
21. **Hooper, D. C., et al.** 1998. Collaboration of antibody and inflammation in clearance of rabies virus from the central nervous system. J. Virol. **72:**3711–3719.
22. **Hornung, V., et al.** 2006. 5′-Triphosphate RNA is the ligand for RIG-I. Science **314:**994–997.
23. **Ito, N., et al.** 2010. Role of interferon antagonist activity of rabies virus phosphoprotein in viral pathogenicity. J. Virol. **84:**6699–6710.
24. **Johnson, N., A. F. Cunningham, and A. R. Fooks.** 2010. The immune response to rabies virus infection and vaccination. Vaccine **28:**3896–3901.
25. **Johnson, N., et al.** 2006. Lyssavirus infection activates interferon gene expression in the brain. J. Gen. Virol. **87:**2663–2667.
26. **Komuro, A., and C. M. Horvath.** 2006. RNA- and virus-independent inhibition of antiviral signaling by RNA helicase LGP2. J. Virol. **80:**12332–12342.
27. **Lafon, M.** 2008. Immune evasion, a critical strategy for rabies virus. Dev. Biol. (Basel) **131:**413–419.
28. **Lafon, M., et al.** 2008. Detrimental contribution of the immuno-inhibitor b7-h1 to rabies virus encephalitis. J. Immunol. **180:**7506–7515.
29. **Lafon, M., et al.** 2005. Modulation of HLA-G expression in human neural cells after neurotropic viral infections. J. Virol. **79:**15226–15237.
30. **Lech, M., A. Avila-Ferrufino, V. Skuginna, H. E. Susanti, and H. J. Anders.** 2010. Quantitative expression of RIG-like helicase, NOD-like receptor and inflammasome-related mRNAs in humans and mice. Int. Immunol. **22:**717–728.
31. **Li, X., et al.** 2009. Structural basis of double-stranded RNA recognition by the RIG-I like receptor MDA5. Arch. Biochem. Biophys. **488:**23–33.
32. **Libeau, G., and M. Lafon.** 1984. Production of monoclonal antibodies against the Pasteur (P.V.) strain of rabies virus: problems and results. Dev. Biol. Stand. **57:**213–218.
33. **Lodmell, D. L., D. L. Wiedbrauk, and L. C. Ewalt.** 1989. Interferon induced within the central nervous system during infection is inconsequential as a mechanism responsible for murine resistance to street rabies virus. J. Gen. Virol. **70:**473–478.
34. **Masatani, T., et al.** 2010. Rabies virus nucleoprotein functions to evade activation of the RIG-I-mediated antiviral response. J. Virol. **84:**4002–4012.
35. **Menager, P., et al.** 2009. Toll-like receptor 3 (TLR3) plays a major role in the formation of rabies virus Negri bodies. PLoS Pathog. **5:**e1000315.
36. **Mendonca, R. Z., and C. A. Pereira.** 1994. Relationship of interferon synthesis and the resistance of mice infected with street rabies virus. Braz. J. Med. Biol. Res. **27:**691–695.
37. **Phares, T. W., R. B. Kean, T. Mikheeva, and D. C. Hooper.** 2006. Regional differences in blood-brain barrier permeability changes and inflammation in the apathogenic clearance of virus from the central nervous system. J. Immunol. **176:**7666–7675.
38. **Pippig, D. A., et al.** 2009. The regulatory domain of the RIG-I family ATPase LGP2 senses double-stranded RNA. Nucleic Acids Res. **37:**2014–2025.
39. **Prehaud, C., F. Megret, M. Lafage, and M. Lafon.** 2005. Virus infection switches TLR-3-positive human neurons to become strong producers of beta interferon. J. Virol. **79:**12893–12904.
40. **Rieder, M., et al.** 2011. Genetic dissection of interferon-antagonistic functions of rabies virus phosphoprotein: inhibition of interferon regulatory factor 3 activation is important for pathogenicity. J. Virol. **85:**842–852.
41. **Rieder, M., and K. K. Conzelmann.** 2009. Rhabdovirus evasion of the interferon system. J. Interferon Cytokine Res. **29:**499–509.
42. **Rothenfusser, S., et al.** 2005. The RNA helicase Lgp2 inhibits TLR-independent sensing of viral replication by retinoic acid-inducible gene-I. J. Immunol. **175:**5260–5268.
43. **Rouse, B. T., and S. Sehrawat.** 2010. Immunity and immunopathology to viruses: what decides the outcome? Nat. Rev. Immunol. **10:**514–526.
44. **Roy, A., and D. C. Hooper.** 2008. Immune evasion by rabies viruses through the maintenance of blood-brain barrier integrity. J. Neurovirol. **14:**401–411.
45. **Roy, A., and D. C. Hooper.** 2007. Lethal silver-haired bat rabies virus infection can be prevented by opening the blood-brain barrier. J. Virol. **81:**7993–7998.
46. **Roy, A., T. W. Phares, H. Koprowski, and D. C. Hooper.** 2007. Failure to open the blood-brain barrier and deliver immune effectors to central nervous system tissues leads to the lethal outcome of silver-haired bat rabies virus infection. J. Virol. **81:**1110–1118.
47. **Satoh, T., et al.** 2010. LGP2 is a positive regulator of RIG-I- and MDA5-mediated antiviral responses. Proc. Natl. Acad. Sci. U. S. A. **107:**1512–1517.
48. **Schreiner, B., et al.** 2004. Interferon-beta enhances monocyte and dendritic cell expression of B7-H1 (PD-L1), a strong inhibitor of autologous T-cell activation: relevance for the immune modulatory effect in multiple sclerosis. J. Neuroimmunol. **155:**172–182.
49. **Smith, J. S., P. A. Yager, and G. M. Baer.** 1973. A rapid tissue culture test for determining rabies neutralizing antibody. Monogr. Ser. World Health Organ. **1973:**354–357.
50. **Strahle, L., et al.** 2007. Activation of the beta interferon promoter by unnatural Sendai virus infection requires RIG-I and is inhibited by viral C proteins. J. Virol. **81:**12227–12237.
51. **Suthar, M. S., et al.** 2010. IPS-1 is essential for the control of West Nile virus infection and immunity. PLoS Pathog. **6:**e1000757.
52. **Thoulouze, M. I., M. Lafage, J. A. Montano-Hirose, and M. Lafon.** 1997. Rabies virus infects mouse and human lymphocytes and induces apoptosis. J. Virol. **71:**7372–7380.
53. **Torres-Anjel, M. J., D. Volz, M. J. Torres, M. Turk, and J. G. Tshikuka.** 1988. Failure to thrive, wasting syndrome, and immunodeficiency in rabies: a hypophyseal/hypothalamic/thymic axis effect of rabies virus. Rev. Infect. Dis. **10**(Suppl. 4)**:**S710–S725.
54. **Venkataraman, T., et al.** 2007. Loss of DExD/H box RNA helicase LGP2 manifests disparate antiviral responses. J. Immunol. **178:**6444–6455.
55. **Vidy, A., M. Chelbi-Alix, and D. Blondel.** 2005. Rabies virus P protein interacts with STAT1 and inhibits interferon signal transduction pathways. J. Virol. **79:**14411–14420.
56. **Vidy, A., J. El Bougrini, M. K. Chelbi-Alix, and D. Blondel.** 2007. The nucleocytoplasmic rabies virus P protein counteracts interferon signaling by inhibiting both nuclear accumulation and DNA binding of STAT1. J. Virol. **81:**4255–4263.
57. **Wang, T., et al.** 2004. Toll-like receptor 3 mediates West Nile virus entry into the brain causing lethal encephalitis. Nat. Med. **10:**1366–1373.
58. **Wang, Z. W., et al.** 2005. Attenuated rabies virus activates, while pathogenic rabies virus evades, the host innate immune responses in the central nervous system. J. Virol. **79:**12554–12565.
59. **Zhao, L., H. Toriumi, Y. Kuang, H. Chen, and Z. F. Fu.** 2009. The roles of chemokines in rabies virus infection: overexpression may not always be beneficial. J. Virol. **83:**11808–11818.